Kim, S., Durand, P., Roques-Carmes, T., Eastoe, J., & Pasc, A. (2015). Metallo-solid lipid nanoparticles as colloidal tools for meso-macroporous supported catalysts. *Langmuir*, *31*(5), 1842-1849. https://doi.org/10.1021/la504708k

Metallo-solid lipid nanoparticles as colloidal tools for meso-macroporous supported catalysts

Sanghoon Kim,[1] Pierrick Durand,[2] Thibault Roques-Carmes,[3] Julian Eastoe,[4] and Andreea Pasc[1]*

[1] Université de Lorraine/CNRS, SRSMC, UMR 7565, F-54506 Vandoeuvre-lès-Nancy, France

[2] Université de Lorraine/CNRS, CRM2, UMR 7036, F-54506, Vandoeuvre-lès-Nancy, France

[3] Université de Lorraine/ENSIC/CNRS, LRGP, UMR 7274, F-54000, Nancy, France

[4] School of Chemistry, University of Bristol, Cantock's Close, Bristol, BS8 1TS, UK

KEYWORDS Meso-macroporous silica, Metallosurfactant, Solid Lipid Nanoparticle, Iron oxide nanoparticle, Fenton-like reaction

ABSTRACT Meso-macroporous silica containing iron oxide nanoparticles (15-20 nm) was synthesized by formulating solid lipid nanoparticles and metallosurfactant as both template and metal source. Due to the high active surface area of the catalyst, the material exhibits an excellent performance in a Fenton-like reaction for methylene blue (MB) degradation, even at low amount of iron oxide (5% TOC after 14h).

INTRODUCTION

In recent years, metal oxides supported on clay,[1-3] silica[4-7] or carbon[8-10] materials have received enormous attention in various fields including heterogeneous catalysis. Among them, silica-supported iron oxide has been intensively studied for wastewater treatment such as degradation of organic dyes through Fenton-like reactions.[11-12] Mesoporous silica has been also widely studied as a support material due to its high pore volume, surface area as well as ordered pore network which provide a good active site accessibility.[13-14] Several studies have proven that iron oxide dispersed in mesoporous silica supports shows not only a considerable improvement of catalytic ability, but also better stability of iron oxide, compared to free iron oxide particles.[15-18] In addition, silica supports combining meso and macroporosity, which bring higher diffusion and throughput rates, could also improve catalytic properties such as reaction rate.[19] Some recent reports have shown the catalytic activity of yolk-shell like structured iron oxide catalysts supported on mesoporous silica with macroporous void spaces.[20-22] Nevertheless, this synthesis requires multiple steps. Moreover, the iron oxide nanoparticles (NPs) have relatively high sizes (~100 nm) and a relative surface/quantity ratio that can still be significantly improved by tailoring NP size.

In this study, we report the preparation of Fe_2O_3@meso-macroporous silica templated with solid lipid nanoparticles (SLNs) and metallosurfactants as iron source, and the application to the degradation of methylene blue (MB) in aqueous solution by a dark Fenton-like reaction initiated by H_2O_2.[23] The key point of this work is that the size of iron oxide nanoparticles embedded in the meso-macroporous matrices has been decreased to 15-20 nm in diameter, to give high surface area of the active catalytic sites in comparison with the previous sub-micron scald iron oxide.[20-

[22, 24] As a matter of fact, these new Fe_2O_3@meso-macroporous silica matrix can successfully degrade the pollutant with twelve-times less iron oxide, than previously reported. [20, 25]

EXPERIMENTAL SECTION

Chemicals: Tetramethylorthosilicate (TMOS), Pluronic P123 and hexadecyltrimethylammonium bromide (CTAB) were purchased from Sigma-Aldrich. N-hexadecylpalmitate (NHP) was purchased from Acros. Ethanol, methanol and Iron (III) chloride ($FeCl_3$) were purchased from Alfa Aesar. Water was deionized and purified using a Milli-Q pack system. All reagents were used without further purification.

Synthesis of metallosurfactant CTAF ($C_{16}H_{33}N(CH_3)_3N^+FeCl_3Br^-$, CetylTrimethyl-Ammonium-trichloromonobromoFerrate): CTAF was synthesized as reported previously.[26] Briefly, 1.77 g of $FeCl_3$ (11.0 mol) was added to 4.0 g of CTAB (11.0 mmol) that was already dissolved in 50 mL of methanol. Then, the solution was heated to reflux overnight. The methanol was evaporated using rotary evaporator and then, the metallosurfactant CTAF was dried *in vacuo* at 60°C for more than 4h.

Preparation of SLN@CTAF: N-hexadecylpalmitate (NHP)-based solid lipid nanoparticles (SLNs) were prepared by the ultra-sonication of hot emulsion method. In ~~a~~ typical procedure, a flask containing 2.2 g of NHP and 20mL of aqueous micellar solution (6.9wt% of Pluronic P123) were heated separately at 70°C. The molten oil phase (NHP) was added to 20 mL of aqueous micellar solution and the mixture was sonicated for 5 min with an ultrasonic device (Branson Sonifier, 60W). After cooling to room temperature under vigorous stirring, 350 mg of metallosurfactant CTAF added to the SLN dispersion and the mixture was kept under stirring for 1 hour.

Synthesis of Fe_2O_3@meso-marcoporous silica material (Silicalization of SLN@CTAF): 0.5 mL of hydrochloric acid (37 wt%) was added to 20 mL of SLN dispersion decorated by CTAF (SLN@CTAF), as prepared above. Then 2.3 g of tetramethylorthosilicate (TMOS) was added dropwise to the solution. The surfactant (P123) / silica precursor (TMOS) molar ratio (R) was 0.016. The mixture was stirred vigorously for 1 hour at room temperature then and was held at 40°C for 24 h, followed by aging at 100°C for 60 h. 'Pasty' as-synthesized silica material was transferred into petri dish and dried *in vacuo* at 30°C for 24 h. 'Dried' as-synthesized silica material was calcinated at 550°C under air (1°C/min) for 6 h.

Catalytic performance of Fe_2O_3@meso-macroporous silica: Fenton-like degradation of MB in aqueous solution was performed with the Fe_2O_3@meso-macroporous silica (denoted as catalyst). 15 mg of catalyst (0.86 mg as Fe_2O_3) was added to a 50 mL beaker containing 20 mL of 50 ppm MB solution. Then the suspension was sonicated for 5 min and kept under stirring at least for 2h to achieve adsorption equilibrium. 1.2 mL of H_2O_2 (30 wt%) was added to initiate the degradation reaction. No acid or base was added for pH adjustment. All reactions were carried out in the dark to avoid the influence of light. At a given interval, 300 µL of solution was withdrawn and quickly centrifuged at 5000 rpm for 10 min to separate silica material. Then 150 µL of solution was diluted to 3mL for UV-Vis measurement (Agilent CARY-3E). The concentration of MB was calculated using standard calibration curve at 664 nm. All data reported are the mean (±) standard deviation of at least three different experiments.

Analyses of methylene blue adsorbed on the catalyst: Methylene blue adsorbed on the catalyst was quantified after 1, 3, 5, 7, 10, 12, 16 and 20 h. The catalyst was first filtered, than dried *in vacuo* at 40°C for 6 h. Then, adsorbed methylene blue was extracted with ethanol (3 x

20mL). The concentration of MB was determined spectrophotometrically using standard calibration curve at 655 nm.

The repeat use of the catalyst: Repeat use of the catalyst was tested in the same conditions as "Catalytic performance of Fe_2O_3@meso-macroporous silica", except that the degradation rate was measured only at 7 h of reaction time. Silica materials were washed with ethanol to remove residual methylene blue, then dried *in vacuo* at 30°C for 24 h before next use.

Characterization: Particle sizing by Dynamic light scattering (DLS) and zeta-potential values were obtained using a Malvern 3000HSA Zetasizer instrument. Nanoparticle tracking analysis (NTA) was performed with Malvern NS300 Nanosight. SAXS measurements were carried out using SAXSee mc^2 (Anton Paar) apparatus. Transmission electron microscopy (TEM) analysis was performed using a Philips CM200 microscope, operated at an accelerating voltage of 200 kV. N_2 adsorption / desorption isotherms were determined on a Micromeritics Tristar 3000 at -196°C. The mesopore size distribution was calculated by the BJH (Barret, Joyner, Halenda) method applied to the adsorption branch of the isotherm. Mercury intrusion porosimetry experiments were performed using Micrometiric AutoPore IV. Macropore size distribution was obtained by applying the Washburn equation to the mercury intrusion curves. ICP-OES elemental analysis was performed on Thermo Fischer ICap 6500. Total organic carbon (TOC) analysis was performed using an Online TOC-VCSH Total Organic Carbon Analyzer (Shimadzu, Japan).

RESULTS AND DISCUSSION

Synthesis of Fe_2O_3@meso-macroporous silica

Fe_2O_3@meso-macroporous silica was prepared (Scheme 1) by adding a silica precursor (tetramethoxylsilane, TMOS) to dispersions of solid lipid nanoparticles stabilized by a metallosurfactant which was added as co-surfactant. The metallosurfactant, $C_{16}H_{33}N(CH_3)_3N^+FeCl_3Br^-$ (CTAF), is simply obtained from cetyltrimethylammonium bromide and iron (III) chloride.[26] Solid lipid nanoparticles were prepared from cetylpalmitate, pluronic P123 and CTAF by the ultra-sonication of hot emulsions followed by solidification.

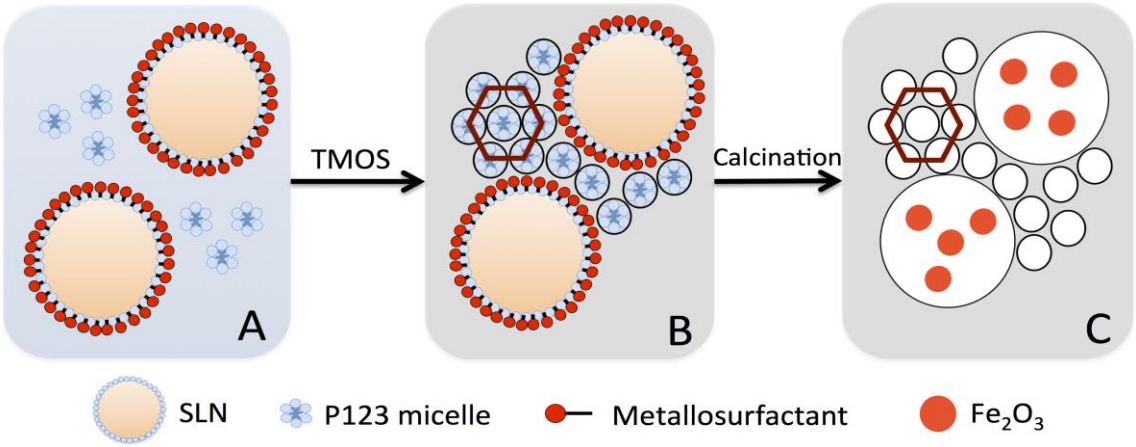

Scheme 1. Synthetic strategy (not to scale): A) CTAF-stabilized solid lipid nanoparticles (SLN) dispersed in micellar P123; B) Silica condensation around SLN, giving hexagonally ordered mesopores; C) Fe_2O_3@meso-macroporous silica obtained by calcination

SLN size distribution was determined using nanoparticle tracking analysis (NTA) and dynamic light scattering (DLS) showing polydisperse populations centered on 160 nm and 230 nm, respectively (Figure 1A and 1B). This size gap is due to the difference between intensity-based measurements in DLS and particle number counting method in NTA. Moreover, by using the fluorescence mode in the NTA, the iron-decorated solid lipid nanoparticles are detected and their size and concentration do not significantly change with respect to those obtained without the filter. The fact that the particles are fluorescent is a direct proof that the iron ions are decorating

the SLN. Also, as control experiment, only $FeCl_3$ was added to a SLN dispersion and measured using a fluorescence filter in the NTA analysis, which gave very weak signal, compared to SLN@CTAF (Supporting information for videos). Indeed, for the $FeCl_3$@SLN system, only weak Fe^{3+}-PEO (pluronic P123) interactions could be expected,[27] which are not strong enough to decorate the SLN interfaces. The adsorption of CTAF at the surface of SLNs was further confirmed by zeta potential measurements. The values of ζ increased with the concentration of CTAF with respect to NHP, until a plateau was reached at 47 mV and 1.8 wt% in metallosurfactant (16wt% of CTAF in NHP/CTAF mixture).

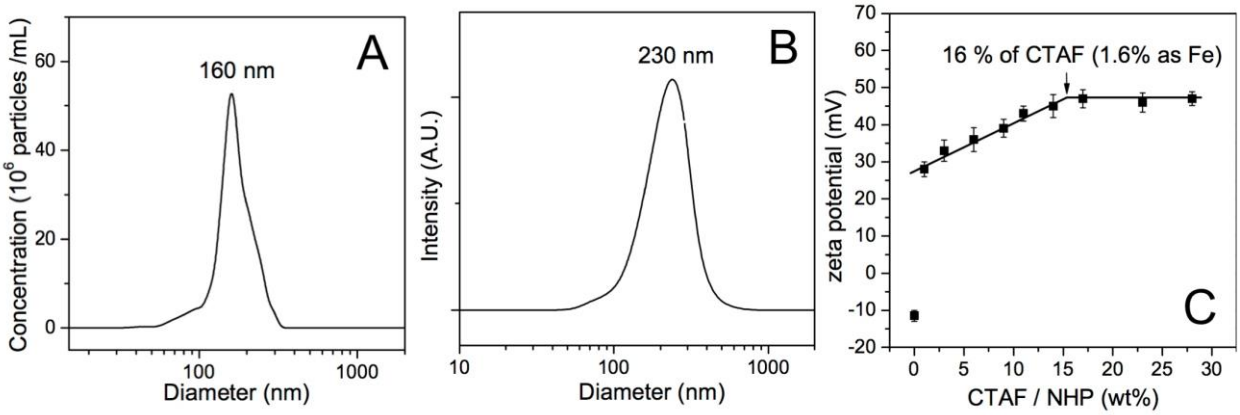

Figure 1. A) Size distribution of SLN@CTAF obtained from NTA (particle number, see Supporting Information for videos); B) Size distribution of SLN@CTAF obtained from DLS (intensity) and C) SLN zeta potential as a function of CTAF level.

By adding TMOS, the dispersions were mineralized through a dual templating mechanism combining micellar cooperativity and templating with the SLNs. The reaction medium was kept at 40°C for 24 h then at 100°C for 24 h to ensure hydrolysis/polycondensation of silica. The obtained 'pasty' as-synthesized material was transferred into a petri dish and dried *in vacuo* at 30°C for 24 h. Then, the material was calcined at 550°C in air to remove the organic matter and to form iron oxide particles, giving the final product, Fe_2O_3@meso-macroporous silica. The

amount of CTAF used to stabilize the SLNs was of 1.8 wt%, which corresponds to the minimum for saturation of the SLN by metallosurfactant.

As shown in Figure 2A, small-angle X-ray scattering (SAXS) analysis indicated that silica materials synthesized with 1.8 wt% CTAF gave, before and after calcination, gave hexagonally ordered mesopores, with three peaks at a characteristic ratio of $1:\sqrt{3}:2$. In the hybrid, as synthesized materials, it can also noticed that the characteristic repeat distance of the solid lipid L□ phase, indicated by (001) reflection position, remains at the same *q* value.[28] Therefore, it seems that CTAF is not intercalating the hexylpalmitate in the core of the SLNs.

N_2 absorption-desorption analysis of Fe_2O_3@meso-macroporous silica showed a type IV isotherm (Figure 2C), which is characteristic of mesoporous materials. The isotherm exhibits a hysteresis loop in accordance of with pore necking, due to the interconnected mesopores. At high relative pressure ($P/P_0 > 0.9$), the N_2 adsorbed volume does not reach a plateau, indicating also the presence of secondary porosity such as macropores. The pore size distribution obtained by the BJH method applied to the adsorption branch isotherm is centered on 7.6 nm (Figure 2D). The BET specific surface area and the mesopore volume are 432 m^2g^{-1} and 0.82 cm^3g^{-1}, respectively.

Interestingly, silica prepared using more than 1.8 wt% of CTAF gave only wormlike materials, with only 1 peak on the diffractogram (Figure 2B). At conc. > 1.8 wt% in CTAF and 6.9 wt% in P123, one can observe by DLS a dual distribution of micelles, centered on 13 nm (mixed P123/CTAF micelles) and 6 nm (CTAF micelles). In this case, the resulting wormlike network exhibits a smaller repetition distance by SAXS (7.7 nm) and smaller pore size as determined by N_2 adsorption/desportion isotherms (5.6 nm). At conc. < 1.8 wt% and 6.9 wt% in P123 the hexagonal structuring of the material is maintained; the repeat distance (Figure 1Bc,d) and the

pore size (Figure SI 1) decrease with the increasing amount of metallosurfactant. This could be explained by the fact that the size of P123 micelles (at 6.9 wt% P123) decreases by adding CTAF from 21 nm to 17 nm (0.6 wt% CTAF), 15 nm (1.2 wt% CTAF), 14 nm (1.8 wt% CTAF). This result could be due to the increase of hydrophilicity of CTAF surfactant that disturbs the self-assembly behavior of P123 micelles.[29-30] This also suggests that the metallosurfactant is indeed distributed between the micelles of P123 forming the mesopores and the surface of SLNs templating the macropores.

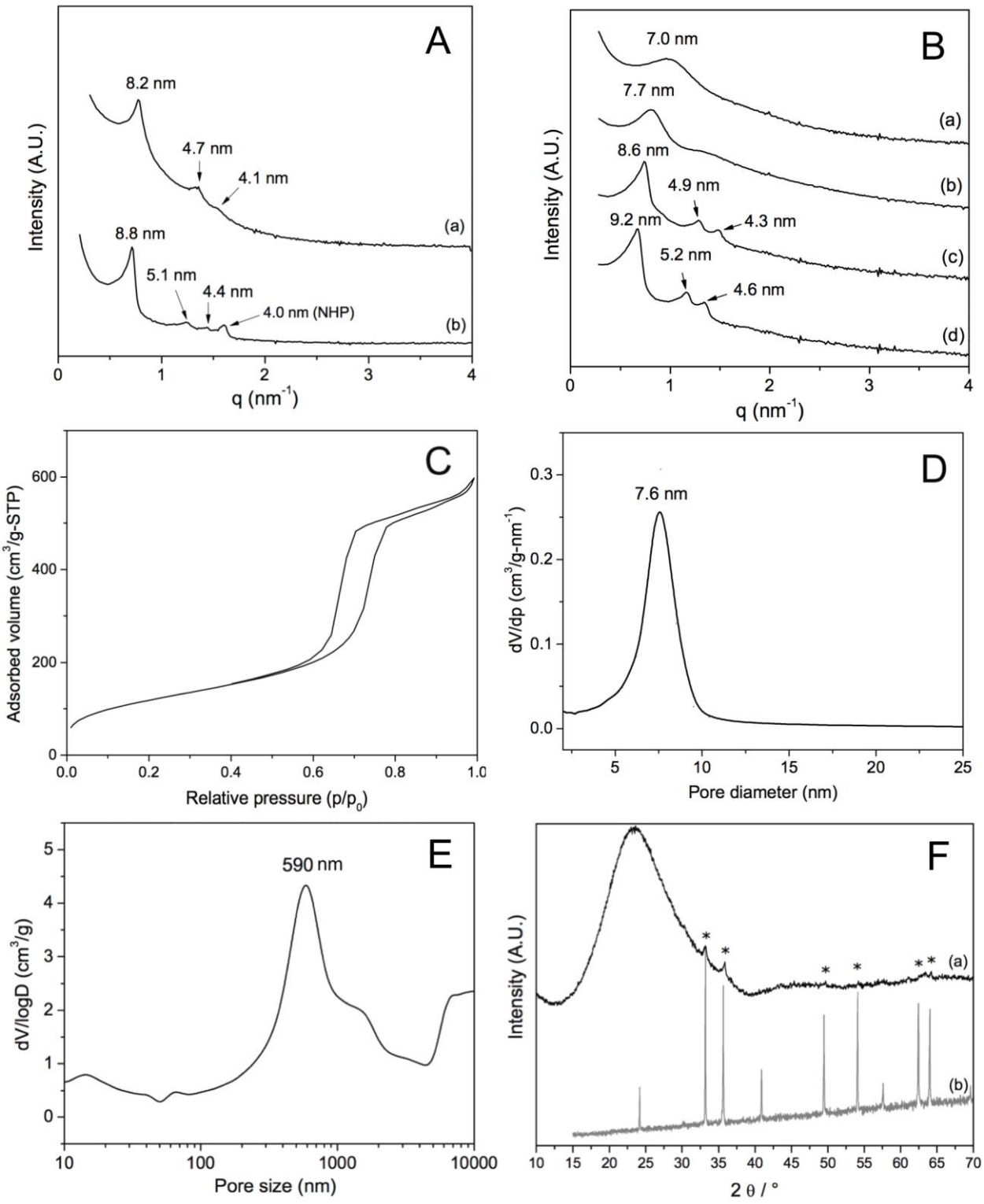

Figure 2. A) SAXS patterns of (a) Fe_2O_3@meso-macroporous silica (the catalyst), (b) as-synthesized material; B) SAXS patterns of meso-macroporous silica prepared with CTAF, (a) 3.0

wt%, (b) 2.4 wt% (c) 1.2 wt% and (d) 0.6 wt%; C) N_2 adsorption–desorption isotherms and D) Pore size distribution of the catalyst; E) Macropore size distribution of the catalyst; F) (a) XRD pattern of the catalyst, (b) Commercial hematite from Sigma-Aldrich

Evidence of the macroporosity was confirmed by mercury intrusion porosimetry experiments (Figure 2E), showing that the macropore size distribution of the material is centered at 590 nm, 2 times larger than the SLNs, with diameters about 230 nm. This could be due to the coalescence of lipid nanoparticles, melted at 100°C during the hydrothermal treatment.[28, 31-32] The mesopore and macropore structures were further confirmed by transmission electron microscopy (TEM) micrographs of Fe_2O_3@meso-macroporous silica, showing macropores with 200-400 nm, interconnected through hexagonally ordered mesopores of about 7.6 nm (Figure 3A). In addition, TEM images indicated the presence of 15-20 nm iron oxide particles encapsulated within the silica matrices. No particles were found on the outer silica surfaces, implying that iron oxide growth occurred exclusively inside the silica matrix.

XRD patterns (Figure 2F) of Fe_2O_3@meso-macroporous silica are characteristic of amorphous silica as evidenced by the broad band around 25°. Small, quite broad peaks are also faintly visible (indicated with an asterix) and are in the same position as crystalline hematite (α-Fe_2O_3). The breadth of the Fe_2O_3 peaks embedded in silica is consistent with nano-sized particles. Using the Scherrer equation[33] and peaks located at 32.8° and at 35.5° give an average size of 15-20 nm, in agreement with the values obtained by TEM.

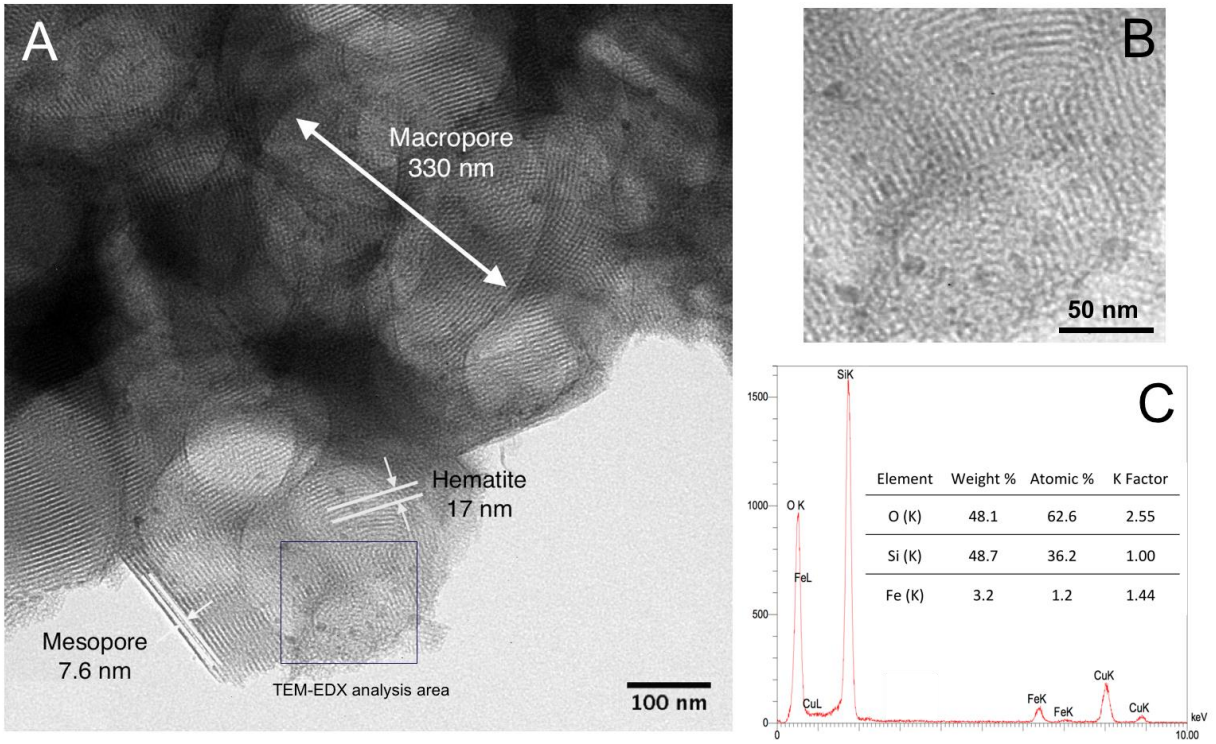

Figure 3. A) TEM image of Fe_2O_3@meso-macroporous silica; B) TEM-EDX analysis area C) TEM-EDX analysis for selected zone

The iron content (4 wt% Fe, 5.7 wt% Fe_2O_3) in Fe_2O_3@meso-macro-porous silica was determined using ICP-OES elemental analysis (Table 1), being in agreement with the TEM-EDX analysis (Figure 3B and 3C).

SiO_2	Al_2O_3	Fe_2O_3	MnO	MgO	CaO	Na_2O	K_2O	TiO_2	P_2O_5	Others	Total
87.23	0.04	5.73	0.02	< DL	< DL	0.02	0.11	< DL	0.24	6.86	100.25

Table 1. ICP-OES elemental analysis (wt%) of Fe_2O_3@meso-macroporous silica

Catalytic performance of Fe_2O_3@meso-macroporous silica

Catalytic performance of Fe_2O_3@meso-macroporous silica was tested through dark Fenton-like degradation of MB in aqueous solution, with H_2O_2 as initiator. Indeed, Fenton-like reactions

are considered as effective advanced oxidation processes (AOPs), which are replacing traditional methods like chlorination, for complete dye degradation in water.[34-35] Fenton-like reactions are based on the catalytic production of hydroxyl radicals, HO·, which can degrade organic compounds under mild conditions.

Although Fenton-like reactions are powerful with almost of iron-based material like iron oxide, rapid scavenging of HO· on the iron oxide surface could limit wide applications. Thus, accessibility of contaminants to the reaction site should be improved using support material such as meso-macroporous silica.[15]

The catalytic assays were performed onto iron oxide@meso-macroporous silica with hexagonally ordered mesopores that has the highest iron content (4.0 wt% Fe), meaning the one obtained with 1.8 wt% of CTAF. The catalysis was performed under similar conditions to those reported by Cui et al[20] (15 mg of silica containing 0.86 mg *vs* 10 mg of Fe_2O_3). As shown in Figure 4A-a, b,c in the absence of the either catalyst or H_2O_2, no dye degradation occurred, showing the decrease of concentration, only due to the adsorption of methylene blue on the catalyst. The extent of adsorption of MB in the bare silica is slightly higher than into Fe_2O_3@silica, that has a smaller surface area (582 m^2/g for bare silica *vs* 432 m^2/g for Fe_2O_3@silica). However, in both cases, the porous catalyst adsorbs 0.053 mg MB/m^2 SiO_2, which is good agreement with the result reported for another mesoporous silica, 0.050 mg/m^2.[36] This phenomenon is well documented in the literature[36] and it is driven by both electrostatic and hydrophobic interactions between the silica surface and the MB.

When the maximum adsorption is reached (t=0) the oxidant is added to the solution. Then, a rapid decrease of methylene blue was observed, as 83% of methylene blue degraded after 7 h (Figure 4A-d). With the catalyst of this work, which contains twelve times less catalyst, the

conversion rate is similar with Cui's catalyst (Figure 4A-e). This gain of performance could be due to the smaller nanoparticle size of Fe_2O_3 (15-20 nm *vs* ~100 nm) having higher active surface/iron content, but also to the presence of interconnected macropores through a mesopore network that provides higher diffusion, throughput, or in other words, a decrease of internal flow resistance.

After 12 h a colourless solution with no UV-Vis signal (Figure 5B-b) was obtained, indicating that all methylene blue in solution had been degraded. Moreover, the extent of MB degradation was examined by total organic carbon (TOC) analysis (Figure 5B-a). The TOC value of the solution was reduced to 23% after 7 h and to less than 5% after 14 h, showing 2.3 mg carbon/L that is close to the mean value of TOC (2.7 mg carbon/L) measured on more than 400 groundwater samples from 8 European Union countries.[37] This result demonstrates that almost no organic by-products were produced during the degradation. For example in water treatment, total degradation of pollutants is very important, because by-products could be more toxic than the pollutants. This is the case of phenol when considering the degradation of MB.[38]

Figure 4D shows the variation of MB adsorbed in the meso-macroporous material with time. The dye was extracted in ethanol and the quantification was by UV analysis. It appears that total degradation of the MB adsorbed in the material is reached after 20 h. Indeed, the catalyst changes color from dark blue (t=0) to green (t=14 h) and finally recovers its original colour, yellowish (t=20h).

Finally, it was investigated the influence of the amount of catalyst on the reaction rate. Up to 7h, methylene blue degradation rate is enhanced as the amount of catalyst increases. The reaction rate could be expressed by a pseudo-first-order model, (Figure 4B) showing an increase in the rate constant (k') with increased amount of catalyst.

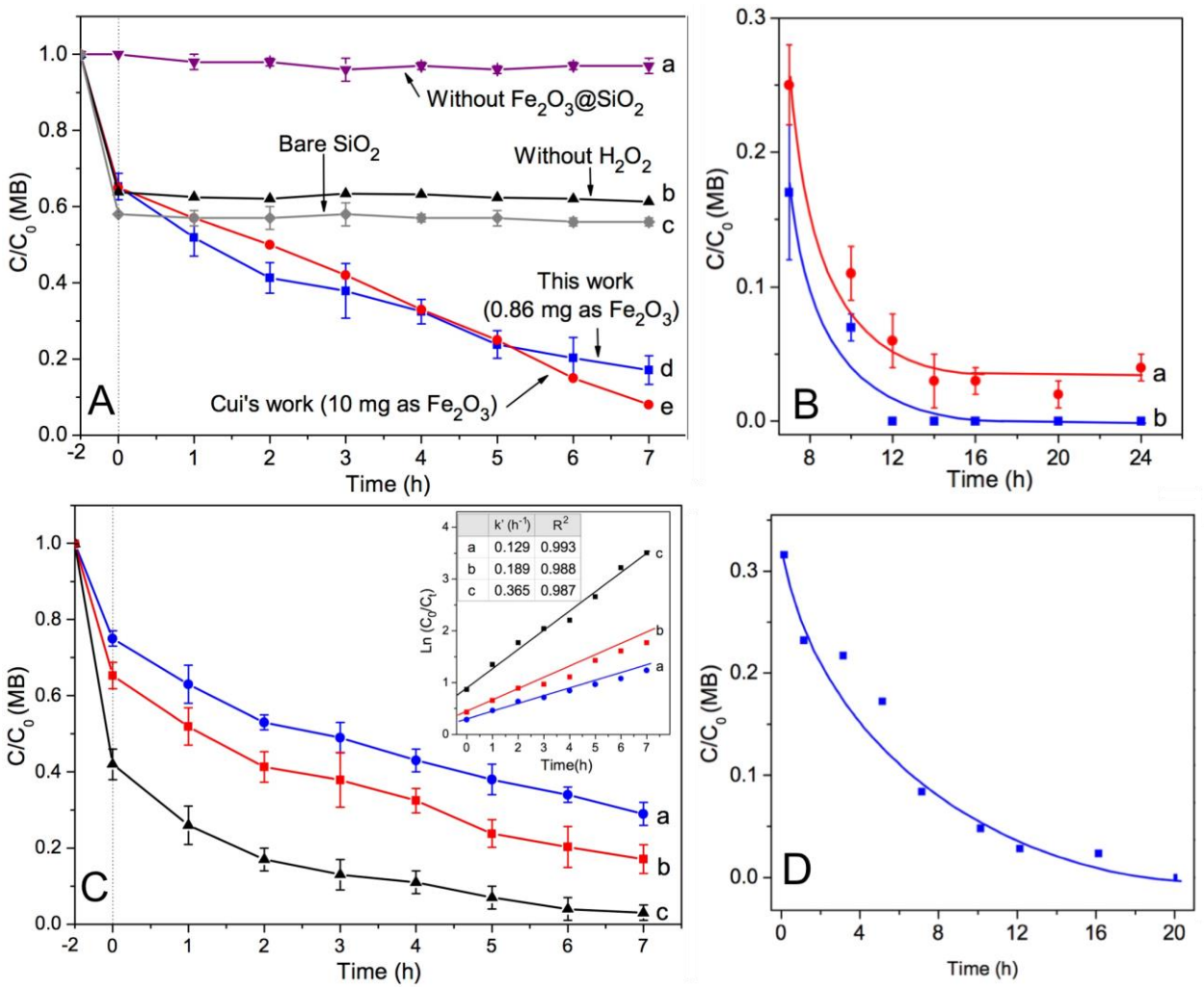

Figure 4. A) Dark Fenton-like degradation of methylene blue in solution, (a) for the blind experiment with only H_2O_2 (without any catalyst), (b) for the catalyst made in this work, without H_2O_2, (c) for bare SiO_2, (d) for the catalyst made in this work, (e) for york-shell structured Fe_2O_3@mesoporous silica (reported by Cui et al.[20]); B) Extended study of methylene blue degradation, using 15mg of catalyst, analysed by (a) UV-Vis and (b) Total Organic Carbon (TOC) measurement; C) Effect of catalyst amount on methylene blue degradation for (a) 10 mg, (b) 15 mg and (c) 30 mg of catalyst, degradation rate fitted using pseudo-first-order model (inset, k' is the rate constant, R^2 is squared correlation coefficient); D) Degradation of methylene blue adsorbed on the catalyst, 15 mg of catalyst used, 32.3% of MB adsorbed before H_2O_2 addition.

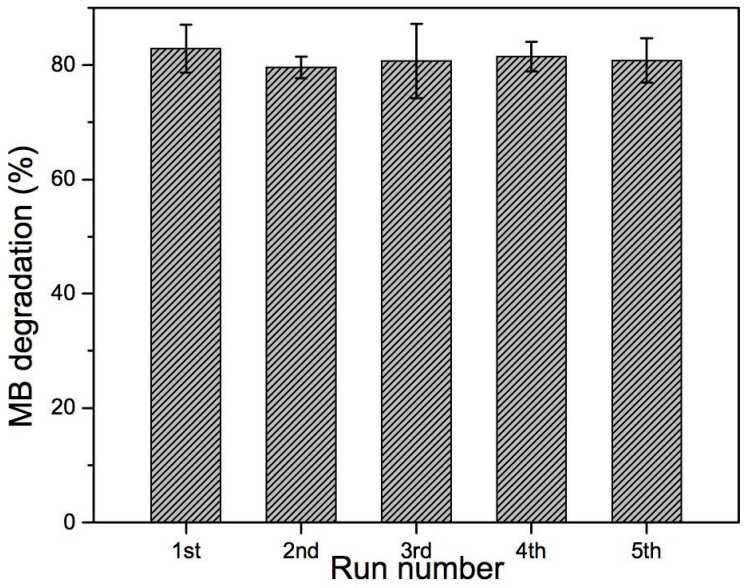

Figure 5. Repeated usability test of catalyst, 15 mg of catalyst used, and all experiments for catalyst reuse were performed for 7 h.

Reusability studies show (Figure 5) that after 5 runs, catalytic performance of the supported catalyst remained quasi-constant (the conversion of MB is of about 83% for 7 h). This result clearly suggests that Fe leaching is limited, due to the silica support and the mild reaction conditions with pH ~ 4.3, in which, Fe_2O_3 solubilisation does not occur.[39] Moreover, SAXS and N_2 adsorption-desorption studies (Figure 6) of the catalyst after 5 runs showed that the mesoporous network remained unaltered, giving 441 m^2g^{-1} as BET specific surface area and 0.87 cm^3g^{-1} as mesopore volume.

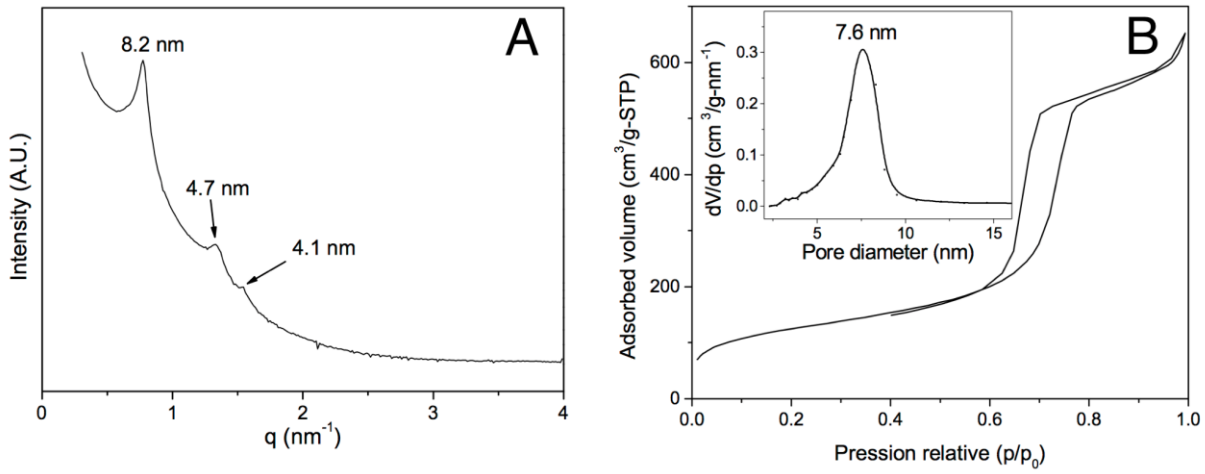

Figure 6. A) SAXS patterns of Fe_2O_3@meso-macroporous silica after 5th use; B) N_2 adsorption–desorption isotherms and pore size distribution (insert) of Fe_2O_3@meso-macroporous silica after 5 runs.

SUMMARY

In conclusion, it has been shown the synthesis of Fe_2O_3 nanoparticles supported in meso-mesoporous silica through a novel and low-cost template, based on solid lipid nanoparticles (SLNs) and iron-containing metallosurfactant. The silica material has hexagonally ordered mesopores and interconnected macropores as well as iron oxide nanoparticles of 15-20 nm in diameter. This Fe_2O_3@meso-macroporous silica showed excellent catalytic activity for dark Fenton-like reactions in methylene blue degradation: complete degradation could be achieved even with a small amount of Fe_2O_3[20, 25], due to high surface area/weight ratio of iron oxide and enhanced diffusion owing to macroporosity. This strategy could be used for other metallic or metal oxide nanoparticles embedded in silica matrices[40-41], for new applications in catalytic processes.

AUTHOR INFORMATION

Corresponding Author

E-mail: andreea.pasc@univ-lorraine.fr; Tel: +33 3 83 68 43 44

Author Contributions

The manuscript was written through contributions of all authors. All authors have given approval to the final version of the manuscript.

Notes

The authors declare no competing financial interest.

ACKNOWLEDGMENT

The authors would like to thank Emmanuel Lamouroux for TEM analysis, Mélanie Emo for X-ray measurements and Steve Pontvianne for TOC analysis. Financial support was received from Institut Jean Barriol and CNRS/University of Lorraine (Project CaMéLIA, PEPS Mirabelle 2014). SK acknowledges the French Minister for Research and Education for the PhD grant. AP acknowledges COST CM1101 network for the STSM grant.

ASSOCIATED CONTENT

Supporting Information. SLN@CTAF tracking analysis videos obtained with NanoSight (Malvern), N_2 adsorption–desorption isotherms and pore size distribution of the material prepared with different amount of CTAF. This material is available free of charge via the Internet at http://pubs.acs.org.

REFERENCES

(1) De Leon, M. A. ; Castiglioni, J.; Bussi, J.; Sergio, M. Catalytic activity of an iron-pillared montmorillonitic clay mineral in heterogeneous photo-Fenton process. *Catal. Today*, **2008**, *133*, 600-605.

(2) Zuo, S.; Huang, Q.; Li, J.; Zhou, R. Promoting effect of Ce added to metal oxide supported on Al pillared clays for deep benzene oxidation. *Appl. Catal., B,* **2009**, *91*, 204-209.

(3) Garrido-Ramirez, E. G.; Theng, B. K. G.; Mora, M. L. Clays and oxide minerals as catalysts and nanocatalysts in Fenton-like reactions - A review. *Appl. Clay Sci*., **2010**, *47*, 182-192.

(4) Huang, Z.; Cui, F.; Kang, H.; Chen, J.; Zhang, X.; Xia, C. Highly Dispersed Silica-Supported Copper Nanoparticles Prepared by Precipitation−Gel Method: A Simple but Efficient and Stable Catalyst for Glycerol Hydrogenolysis. *Chem. Mater*., **2008**, *20*, 5090-5099.

(5) Jiao, F.; Frei, H. Nanostructured Cobalt Oxide Clusters in Mesoporous Silica as Efficient Oxygen-Evolving Catalysts. *Angew. Chem. Int. Ed.,* **2009**, *48*, 1841-1844.

(6) Horzum, N.; Munoz-Espi, R.; Glasser, G.; Demir, M. M.; Landfester, K.; Crespy, D. Hierarchically Structured Metal Oxide/Silica Nanofibers by Colloid Electrospinning. *ACS Appl. Mater. Interfaces*, **2012**, *4*, 6338-6345.

(7) Kobayashi, K.; Kitaura, R.; Kumai, Y.; Goto, Y.; Inagaki, S.; Shinohara, H. Fabrication of single-wall carbon nanotubes within the channels of a mesoporous material by catalyst-supported chemical vapor deposition. *Carbon*, **2009**, *47*, 722-730.

(8) Chen, W.; Pan, X.; Williger, M.; Su, D. S.; Bao, X. Facile Autoreduction of Iron Oxide/Carbon Nanotube Encapsulates. *J. Am. Chem. Soc.*, **2006**, *128*, 3136-3137.

(9) Sun, Z.; Sun, S.; Qiao, M.; Wei, J.; Yue, Q.; Wang, C.; Deng, Y.; Kaliaguine, S.; Zhao, D. A General Chelate-Assisted Co-Assembly to Metallic Nanoparticles-Incorporated Ordered Mesoporous Carbon Catalysts for Fischer–Tropsch Synthesis. *J. Am. Chem. Soc*., **2012**, *134*, 17653-17660.

(10) Su, D. S.; Perathoner, S.; Centi, G. Nanocarbons for the Development of Advanced Catalysts. *Chem. Rev.,* **2013**, *113*, 5782-5816.

(11) Ferroudj, N.; Nzimoto, J.; Davidson, A.; Talbot, D.; Briot, E.; Dupuis, V.; Bée, A.; Medjram, M. S.; Abramson, S. Maghemite nanoparticles and maghemite/silica nanocomposite microspheres as magnetic Fenton catalysts for the removal of water pollutants. *Appl. Catal., B*, **2013**, *136*, 9-18

(12) Botas, J. A.; Melero, J. A.; Martinez, F.; Pariente, M. I. Assessment of Fe_2O_3/SiO_2 catalysts for the continuous treatment of phenol aqueous solutions in a fixed bed reactor. *Catal. Today*, **2010**, *149*, 334-340.

(13) Zhang, H.; Bandosz, T. J.; Akins, D. L. Template-free synthesis of silica ellipsoids. *Chem. Commun*., **2011**, *47*, 7791-7793.

(14) Srinivasan, N.R.; Bandyopadhyaya, R. Highly accessible SnO_2 nanoparticle embedded SBA-15 mesoporous silica as a superior photocatalyst. *Microporous Mesoporous Mater*., **2012**, *149*, 166-171.

(15) Pham, A. L.-T.; Lee, C.; Doyle, F. M.; Sedlak, D. L. A Silica-Supported Iron Oxide Catalyst Capable of Activating Hydrogen Peroxide at Neutral pH Values. *Enviro. Sci. Technol*., **2009**, *43*, 8930-8935.

(16) Li, Y.; Chen, Y.; Li. L.; Gu, J.; Zhao, W.; Li, L.; Shi, J. A simple co-impregnation route to load highly dispersed Fe(III) centers into the pore structure of SBA-15 and the extraordinarily high catalytic performance. *Appl. Catal., A*, **2009**, *366*, 57-64.

(17) Ursachi, I.; Stancu, A.; Vasile, A. Magnetic α -Fe_2O_3/MCM-41 nanocomposites: Preparation, characterization, and catalytic activity for methylene blue degradation. *J. Colloid Interface Sci.,* **2012**, *377*, 184-190

(18) Soon A. N.; Hameed, B. H. Degradation of Acid Blue 29 in visible light radiation using iron modified mesoporous silica as heterogeneous Photo-Fenton catalyst. *Appl. Catal., A,* **2013**, *450*, 96-105.

(19) Parlett, C. M. A.; Winson, K.; Lee, A. F. Hierarchical porous materials: catalytic applications. *Chem. Soc. Rev*., **2013**, *42*, 3876-3893.

(20) Cui, Z. M.; Chen, Z.; Cao, C. Y.; Jiang, L.; Song, W. G. A yolk–shell structured Fe_2O_3@mesoporous SiO_2 nanoreactor for enhanced activity as a Fenton catalyst in total oxidation of dyes. *Chem. Commun*., **2013**, *49*, 2332-2334.

(21) Castillo, S. I. R.; Pompe, C. E.; van Mourik, J.; Berbart, D. M. A.; Thies-Weesie, D. M. E.; de Jongh, P. E.; Philipse, A. P. Colloidal cubes for the enhanced degradation of organic dyes. *J. Mater. Chem. A*, **2014**, *2*, 10193-10201.

(22) Zeng, T.; Zhang, X.; Wang, S.; Ma, Y.; Nui, H.; Cai, Y. Assembly of a Nanoreactor System with Confined Magnetite Core and Shell for Enhanced Fenton-Like Catalysis. *Chem. Eur. J*., **2014**, *20*, 6474-6481.

(23) Neyens, E.; Baeyens, J. A review of classic Fenton's peroxidation as an advanced oxidation technique. *J. Hazard. Mater*., **2003**, *98*, 33-50.

(24) Martínez, F.; Calleja, G.; Melero, J. A.; Molina, R, Heterogeneous photo-Fenton degradation of phenolic aqueous solutions over iron-containing SBA-15 catalyst. *Appl. Catal., B,* **2005**, *60*, 181-190.

(25) Vu, T. T.; Marban, G. Sacrificial template synthesis of high surface area metal oxides. Example: An excellent structured Fenton-like catalyst. *Appl. Catal., B,* **2014**, *152*, 51-58.

(26) Kim, S.; Bellouard, C.; Pasc, A.; Lamouroux, E.; Blin, J.-L.; Carteret, C.; Fort, Y.; Emo, M.; Durand, P.; Stébé, M. J. Nanoparticle-free magnetic mesoporous silica with magneto-responsive surfactants. *J. Mater. Chem. C*, **2013**, *1*, 6930-6934.

(27) Zhang, R.; Dai, H.; Du, Y.; Zhang, L.; Deng, J.; Xia, Y.; Zhao, Z.; Meng, X.; Lui, Y. P123-PMMA Dual-Templating Generation and Unique Physicochemical Properties of Three-Dimensionally Ordered Macroporous Iron Oxides with Nanovoids in the Crystalline Walls. *Inorg, Chem*, **2011**, *50*, 2534-2544.

(28) Kim, S.; Stébé, M. J.; Blin, J.-L.; Pasc, A. pH-controlled delivery of curcumin from a compartmentalized solid lipid nanoparticle@mesostructured silica matrix. *J. Mater. Chem. B,* **2014**, *2*, 7910-7917.

(29) da Silva, R. C.; Olofsson, G.; Schillén, K.; Loh, W.; Influence of Ionic Surfactants on the Aggregation of Poly(Ethylene Oxide)−Poly(Propylene Oxide)−Poly(Ethylene Oxide) Block Copolymers Studied by Differential Scanning and Isothermal Titration Calorimetry. *J. Phys. Chem. B*, **2002**, *106*, 1239-1246.

(30) Zhang, W. -H.; Zhang, L.; Xiu, J.; Shen, Z.; Li, Y.; Ying, P.; Li, C. Pore size design of ordered mesoporous silicas by controlling micellar properties of triblock copolymer $EO_{20}PO_{70}EO_{20}$. *Microporous Mesoporous Mater.,* **2006**, *89*, 179-185.

(31) Pasc, A.; Blin, J.-L.; Stébé, M. J.; Ghanbaja, J. Solid lipid nanoparticles (SLN) templating of macroporous silica beads. *RSC Advances*, **2011**, *1*, 1204-1206.

(32) Ravetti-Duran, R.; Blin, J.-L.; Stébé, M. J.; Castel, C.; Pasc, A. Tuning the morphology and the structure of hierarchical meso–macroporous silica by dual templating with micelles and solid lipid nanoparticles (SLN). *J. Mater. Chem*., **2012**, *22*, 21540-21548.

(33) Holzwarth, U.; Gibson, N. The Scherrer equation versus the 'Debye-Scherrer equation. *Nature Nanotech*, **2011**, *6*, 534.

(34) Oturan, M. A.; Aaron, J.-J.; Advanced Oxidation Processes in Water/Wastewater Treatment: Principles and Applications. A Review. *Crit. Rev. Environ. Sci. Technol.*, **2014**, *44*, 2577-2641.

(35) Ensing, J.; Buda, F.; Baerends, E. J.; Fenton-like Chemistry in Water: Oxidation Catalysis by Fe(III) and H_2O_2. *J. Phys. Chem. A.*, **2003**, *107*, 5722-5731.

(36) Ho, K. Y.; McKay, G. Yeung, K. L.; Selective Adsorbents from Ordered Mesoporous Silica. *Langmuir*, **2003**, *19*, 3019-3024.

(37) Gooddy, D.C.; Hinsby, K. Organic Quality of Groundwaters, in Natural Groundwater Quality (W.M. Edmunds, P. Shand), Wiley-Blackwell Publishing, Ltd, **2008**, Oxford, UK.

(38) Houas, A.; Lachbeb, H.; Ksibi, M.; Elaloui, E.; Guillard, C.; Herrmann, J. Photocatalytic degradation pathway of methylene blue in water. *Appl. Catal., B,* **2001**, *31*, 145-157.

(39) Jang, J.; Dempsey, B. A.; Burgos, W. D. Solubility of Hematite Revisited: Effects of Hydration. *Environ. Sci. Technol*., **2007**, *41*, 7303-7308.

(40) Strunk, J.; Vining, W. C.; Bell, A. T., Synthesis of Different CeO_2 Structures on Mesoporous Silica and Characterization of Their Reduction Properties, *J. Phys. Chem. C*, **2011**, *115*, 4114–4126.

(41) Xu, Y.; Chen, D.; Jiao, X.; Xue, K., Nanosized Cu_2O/PEG400 Composite Hollow Spheres with Mesoporous Shells, *J. Phys. Chem. C*, **2007**, *111*, 16284–16289.

Table of Contents Graphic